2nd Symposium on New Trends in Nuclear and Medical Physics, Poland, September 24–26, 2025

Fragmentation Measurements for Particle Therapy with the FOOT Experiment

A.C. Kraan[a,*] (on Behalf of the FOOT Collaboration)

[a]*National Institute for Nuclear Physics (INFN), Pisa Division, Edificio C — Polo Fibonacci Largo B. Pontecorvo 3, 56127 Pisa, Italy*

Doi: 10.12693/APhysPolA.148.S145 *e-mail: aafke.kraan@pi.infn.it

FOOT (FragmentatiOn Of Target) is an innovative experiment in applied nuclear physics, dedicated to the understanding of nuclear fragmentation processes. This is relevant in oncological treatments with hadron beams and in the field of radiation protection in space. The FOOT physics program foresees a set of measurements conducted in both direct and inverse kinematics, employing particle beams and targets relevant to particle therapy and radiation protection in space. The main goal of the experiment is to measure double differential cross sections as a function of scattering angle and fragment energy within the 100–800 MeV/u range, achieving a precision level exceeding 5%. Currently, the FOOT collaboration has developed two experimental setups, i.e., one based on nuclear emulsions, designed for charges $Z \leq 3$, and another based on electronic detectors, for fragments with $Z \geq 2$. In this contribution, we first discuss the physical motivations of the experiment, followed by an overview of the apparatus. Then, some preliminary and recent results are presented, highlighting a few specific issues, such as charge identification, recent results with helium beams, and recent cross-section measurements. Finally, the upcoming experimental campaigns will be discussed.

topics: FOOT (FragmentatiOn Of Target), particle therapy, nuclear interactions, charge identification

1. Introduction

Particle therapy is an external beam radiotherapy technique that primarily uses charged particles, such as protons, carbon ions, and, more recently, helium ions, to treat tumors [1–4]. Compared to conventional radiotherapy, particle therapy allows for more conformal dose distributions, thanks to the Bragg peak of charged particles. While its clinical use is expanding, further research is needed to enhance its accuracy [3, 5, 6]. An important research topic is reducing the uncertainty of the radiobiological effectiveness (RBE) of particle beams (see, for example, [2, 7–9]), which is essential for accurate biological dose calculations and better prediction of treatment outcomes. RBE depends on several physical and biological factors, including the spectrum of nuclear fragments produced when the beam interacts with patient tissue. Accurate modeling of fragment production is crucial for treatment planning but remains difficult due to the energies involved, namely from 50 to 250 MeV for protons and from 100 to 450 MeV/u for carbon ions. In this range, theoretical models often fall short. Experimental data, particularly double differential cross sections in energy and angle with thin targets, are needed to improve these models [10, 11]. At present, such measurements are limited and available only for a few projectiles and energies, as emphasized in several recent reviews [10–12].

Apart from particle therapy, these types of measurements, performed at higher energies, are also important for radioprotection in space [11, 12]. Neutrons and light ions ($Z = 1$, $Z = 2$) are the most important secondary particles produced in space radiation, with energies ranging from a few hundred MeV to several GeV. Particles of these energies can penetrate deeply, making large contributions to the dose. Transport codes require double differential cross sections, including large angles, to accurately model how the radiation propagates through shielding and human tissue. This is particularly important for long-term missions in space.

The FOOT experiment will measure with great precision (about 5%) the nuclear fragmentation cross section of medium-light ions such as protons, helium, carbon, and oxygen, in thin tissue-like targets (graphite, polyethylene) [13]. The collaboration has constructed a compact and portable setup that fits in the typically limited space of particle therapy treatment centers, where most data collection occurs, including the National Center for Oncological Hadrotherapy (CNAO) in Pavia, Italy, Helmholtz Zentrum für Schwerionenforschung (GSI) in Darmstadt, Germany, and Heidelberger

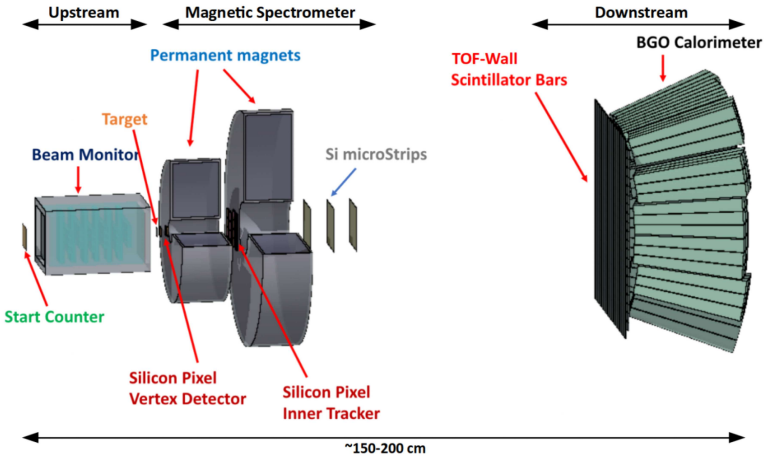

Fig. 1. Schematic view of electronic setup (from left): the upstream, magnetic spectrometer, and downstream regions. Adapted from [13] with permission (CC-BY licence).

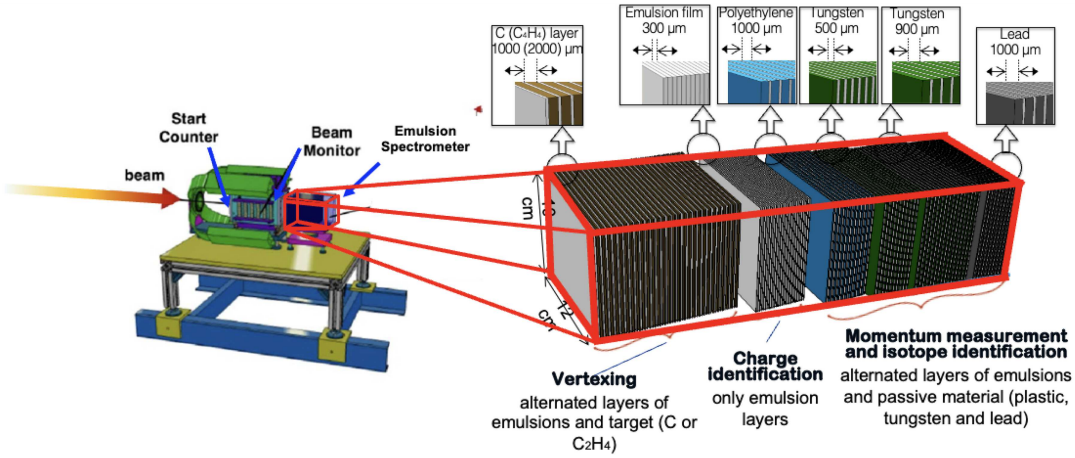

Fig. 2. Schematic view of the emulsion spectrometer. Adapted from [13, 14] with permission.

Ionenstrahl-Therapiezentrum (HIT) in Heidelberg, Germany. Two distinct experimental setups have been constructed, i.e., an electronic setup for particles with $Z \geq 2$ and an emulsion spectrometer for particles with $Z \leq 3$.

Below, we will first describe the strategy and experimental apparatus. We will then present a selection of results, with a focus on some specific aspects of the electronic setup, such as the role of the TOF-wall (TW) in charge identification and recent cross-section measurements.

2. FOOT experimental setup

2.1. Design and inverse kinematics approach

The FOOT experiment is primarily funded by the National Institute for Nuclear Physics (Italy) and consists of about a hundred researchers from Italian and foreign institutes. The experimental design and first results of performance are discussed in detail in [13]. The design includes two complementary setups. The electronic setup focuses on heavier fragments ($Z \geq 2$) that are forward-peaked within $\sim 10°$. The emulsion spectrometer setup is used for lighter fragments ($Z \leq 3$) that typically spread up to 50–60°. The two setups share the pre-target (upstream) region, aimed at monitoring the primary beam. They differ in the downstream region, which is dedicated to fragment tracking and identification. Schematics of the electronic and the emulsion setups are given in Figs. 1 and 2, respectively. This contribution mostly focuses on the electronic setup, described below. The emulsion spectrometer has been described in detail by Galati et al. [14]. The typical beam rate at which the experiment operates is low (< 10–20 kHz) — much lower than typical particle therapy beam rates.

In nuclear physics interactions, we can distinguish between target and projectile fragmentation (see Fig. 3). Target fragments, particularly relevant in proton–nucleus interactions, typically have low

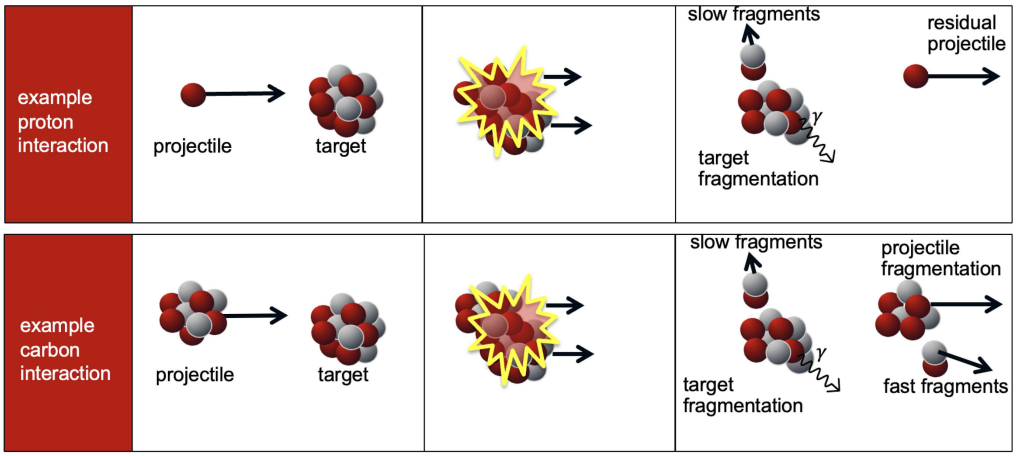

Fig. 3. Target fragmentation and projectile fragmentation in a proton and a carbon ion interaction.

energies and short ranges (10–100 μm in tissue) due to their high linear energy transfer (LET). As a result, even thin targets tend to stop most of these fragments, making energy measurement difficult. The inverse kinematics approach is used to solve this issue, where heavier ion beams (e.g., ^{12}C, ^{16}O) collide with hydrogen-rich targets, reversing the roles of projectile and target. The two configurations can be related by a Lorentz boost. Fragments produced in inverse kinematics are much more energetic and can exit the target, making detection feasible.

2.2. Upstream region

The upstream (pre-target) region (Fig. 1) tracks the primary beam and provides the start time for time-of-flight (TOF) measurements. It consists of:

- Start counter (SC), which is the first detector encountered by the beam. It is a 5×5 cm^2 large and 250 μm-thick EJ-200 plastic scintillator foil, housed in an aluminum frame within a light-tight box with aluminized mylar layers [15]. The thin design ensures minimal beam interaction while achieving $\sim$ 50 ps time resolution. It is read out by 48 Hamamatsu 3×3 cm^2 silicon photomultipliers (SiPMs), grouped into 8 channels. The SC monitors the beam rate, provides the minimum bias trigger, serves as a time reference for all detectors, and marks the TOF start time.
- Beam monitor (BM), located between the SC and the target. It is a drift chamber filled with an Ar/CO_2 (80%/20%) gas mix [16]. It has a 5.6×5.6 cm^2 active area and 12 layers of alternating horizontal and vertical wires. The BM determines the beam direction and impact point on the target, essential for resolving pile-up in downstream detectors and identifying out-of-target events. Proton beam tests have shown 93% hit efficiency and spatial resolution better than 100 μm in the central region, enabling angular precision of a few milliradians.

2.3. Magnetic spectrometer region

The beam then passes through the target, which is typically a thin (5 mm) plate of carbon or polyethylene, housed in a mechanical structure. The detectors in the magnetic spectrometer region are for particle tracking and momentum measurement. The beam passes through the following structures:

- Vertex detector (VTX), consisting of two substations, each with two layers of MIMOSA-28 (M28) CMOS Monolithic Active Pixel Sensors. Positioned 0.5 cm from the target, the VTX stations are separated by 10 mm, with 2 mm between chips. It provides a 5 μm spatial resolution for vertex reconstruction.
- Magnet system (MS), including two cylindrical permanent magnets with bore radius of 3 and 5 cm, respectively, and external radius 15 and 23 cm, respectively. They are spaced 5 cm apart. Each magnet is made of Nd–Fe–Co modules in a Hallbach configuration, generating a near-uniform dipolar field inside. The magnets (200–300 kg) produce peak magnetic fields of 1.3 and 0.9 T, respectively, and can be vertically displaced. The magnet is described in detail in [17].
- Inner tracker (IT), located in between the two magnets. The distance from the target is roughly 20 cm. It includes two planes of 16 M28 chips, arranged in double-sided ladders on aluminum frames, covering an 8×8 cm^2 area. The IT determines the track direction and transverse position within the magnetic field.

- Microstrip silicon detector (MSD), positioned about 35 cm from the target. It consists of three stations of six single-sided silicon detectors, 150 μm-thick, in alternating orthogonal layers, spaced 4–5 cm apart. Each detector has a 9.6×9.3 cm^2 active area. The MSD performs fragment tracking for momentum measurement and charge identification via $\mathrm{d}E/\mathrm{d}x$. Tests with protons, ^{12}C, and ^{16}O beams have shown a spatial resolution from 10–35 μm [18].

2.4. Downstream region

Located about 1 m from the target, the downstream region provides the final timestamp for TOF measurements and measures the energy loss for fragment charge and mass identification. The key elements of the downstream configuration are:

- The TOF-wall (TW) consists of two orthogonal layers of 20 EJ-200 plastic scintillator bars (0.3 cm thick, 2 cm wide, 44 m long), forming a 40×40 cm^2 active area with 2×2 cm^2 granularity. Each bar is read at both ends by four Hamamatsu MPPC SiPMs (3×3 mm^2, 25 μm pitch). The SiPMs detect scintillation light to measure TOF and energy loss (ΔE). The energy and TOF resolution of TW are $< 5\% \Delta E$ and 70 ps, respectively. Along the bar, the position resolution is about 8 mm. Together with the SC, the TW forms the ΔE–TOF system, crucial for charge identification (see Fig. 4). Details of the detector are given in [19, 20].
- BGO calorimeter (CALO). Positioned at the far end, the calorimeter consists of 32 modules of 24 cm long bismuth germanate (BGO) crystals arranged in 3×3 blocks. Details are given in [21]. The geometry is displayed in Fig. 5. Each crystal, shaped as a truncated pyramid (2×2 cm^2 front, 2.9×2.9 cm^2 back), is read by a 5×5 SiPM matrix (15 μm pitch). BGO was chosen for its high density (7.13 g/cm^3) and light yield ($\sim$ 10 photons/keV), offering $< 2\%$ energy resolution for mass identification. The response time is about 300 ns.

2.5. DAQ, trigger and analysis

The FOOT data acquisition (DAQ) chain is a hierarchical, distributed system using Linux PCs, VME crates, detector readouts, and communication via Ethernet, USB, and optical fibers. A more detailed description of the design is available in [22]. To efficiently select events (only about 1 in 100 events is a fragmentation), two triggers are used, namely a minimum bias (MB) trigger, fired when

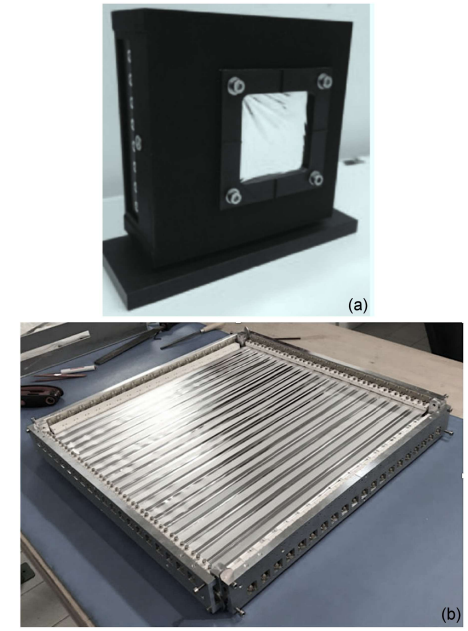

Fig. 4. Pictures of the detectors involved in the ΔE–TOF system: (a) SC and (b) TW.

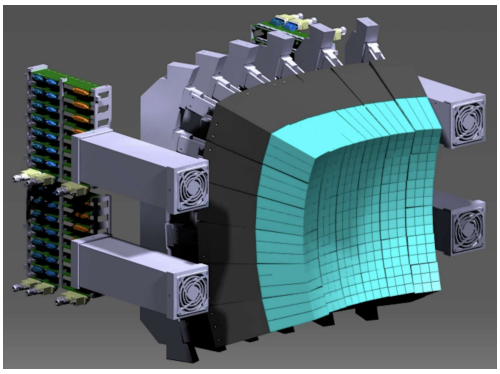

Fig. 5. FOOT calorimeter. Reproduced from [21].

≥ 5 SC channels are hit, and a fragmentation trigger (FRAG), adding the condition that hits are detected in the central TW bars. The SC, TW, and calorimeter signals are digitized by WaveDAQ, using custom WaveDREAM boards (WDBs), sampling up to 5 Gsamples/s with 16-bit analog-to-digital converters (ADCs). Analysis is performed with dedicated software named SHOE.

2.6. Present status

All the detectors mentioned above are now constructed. Most of them have been tested and characterized on several occasions, including CNAO, GSI, and HIT. Reconstruction and analysis software has also been developed.

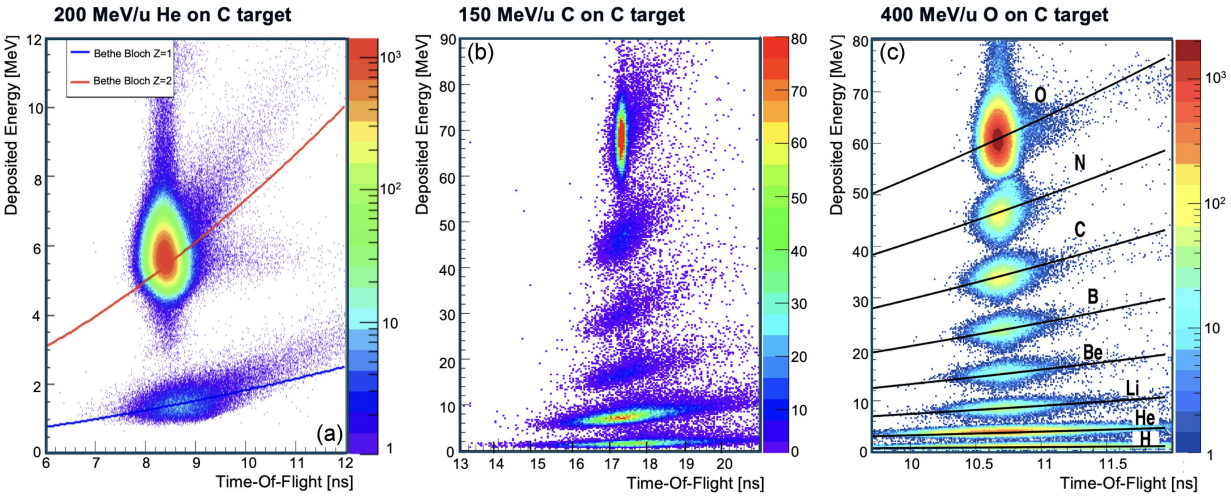

Fig. 6. Examples of ΔE–TOF distributions of nuclear fragments produced in a 5 mm carbon target by a 150 MeV carbon beam (a), a 400 MeV oxygen beam (b), and a 200 MeV helium beam (c) in the TW. The figure in (c) was adapted from [24], with permission, while (a) was obtained from [23].

3. Results

3.1. Charge identification

The TW energy and TOF are calibrated by equalizing with MC simulations [19, 20]. Resolutions in TOF and resolutions in deposited energy ΔE in the bars were determined on various occasions with monoenergetic beams without a target at CNAO, HIT, and GSI [19, 20, 23]. The resulting Z resolutions for several charged particles were also determined [20, 23] and are summarized in Table I. The Z resolutions depend on the particle type and energy. They also depend on the SiPM gain, which was not the same on all occasions.

Examples of ΔE–TOF distributions of data with a target are given in Fig. 6, where panel (a) represent nuclear fragments produced by a 200 MeV helium beam on a 5 mm carbon target at HIT (presented in [23]), panel (b) shows a 150 MeV carbon beam on a 5 mm thick carbon target at CNAO, and panel (c) — a 400 MeV oxygen beam on a 5 mm thick carbon target at GSI, as published by Ridolfi et al. [24]. The nuclear fragments with different charge Z can clearly be distinguished.

TABLE I

Results for the Z resolution for a given facility (first column), particle type (second column), beam energy (third column), mean Z value ($\mu(Z)$, fourth column), Z resolution ($\sigma(Z)$, fifth column), and relative Z resolution (R_Z, sixth column). Note that all values are rounded to two decimal places. These results were obtained with monoenergetic beams without a target. Data were extracted and combined from [20, 23]. Note that some of the results were obtained on different occasions and that the detector settings were not always identical.

Facility	Particle	Beam energy [MeV/u]	$\mu(Z)$	$\sigma(Z)$	R_Z [%]
CNAO	p	60	0.96	0.06	6.10
HIT	He	100	2.03	0.06	2.72
HIT	He	140	2.04	0.07	3.44
HIT	He	200	2.06	0.09	4.36
HIT	He	220	2.05	0.09	4.51
CNAO	^{12}C	115	6.17	0.15	2.51
CNAO	^{12}C	260	6.01	0.21	3.52
CNAO	^{12}C	400	6.07	0.24	3.85
GSI	^{16}O	400	8.07	0.22	2.67

3.2. Angular cross-section measurements

Recently, FOOT has measured angular differential and elemental fragmentation cross sections of a 400 MeV/nucleon ^{16}O beam on a graphite target [24]. In the experimental setup, only the SC, BM, and TW detectors were present. Beam particles and fragments were tracked and identified by the TOF and ΔE only. The fragment angle was determined by the granularity of the TW. The elemental cross section for each fragment charge was computed as [24]

$$\frac{\mathrm{d}\sigma}{\mathrm{d}\Omega}(Z,\theta) = \frac{N_{\mathrm{frag}}(Z,\theta)}{N_{\mathrm{prim}}\, n_t\, \epsilon(Z,\theta)\Delta\Omega}, \qquad (1)$$

where N_{frag} is the selected number of fragments of a given charge Z measured by TW at a given angle θ, N_{prim} is the number of primaries impinging on

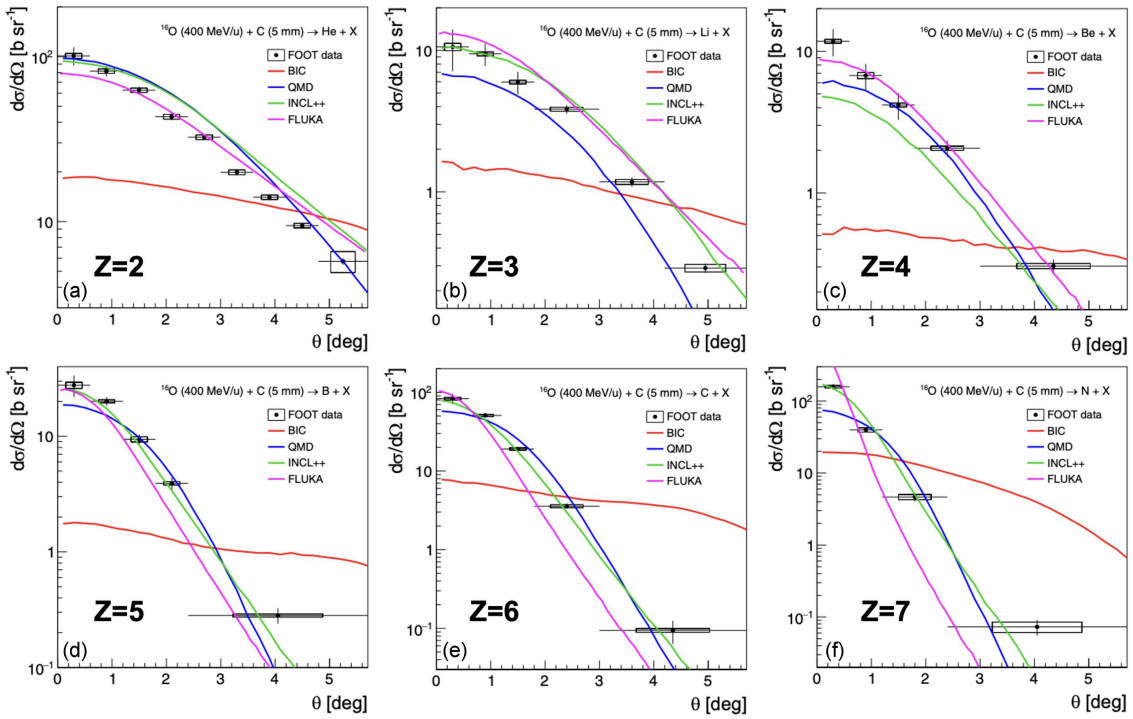

Fig. 7. Angular differential cross sections for the production of He, Li, Be, B, C, and N fragments in nuclear interactions of a 400 MeV/u ^{16}O beam on a 5 mm graphite target, together with predictions from four different models: BIC (red), QMD (blue), INCL++ (green), and FLUKA (pink). Adapted from [24], with permission.

the target, $\epsilon(Z,\theta)$ is the efficiency for a given fragment with charge Z to be reconstructed correctly for a given angle, computed using the FLUKA MC code, $\Delta\Omega$ is the solid angle bin width, and n_t is the number of interaction centers in the target per unit surface. For each species (He, Li, Be, B, C, N), the yields were determined and binned in scattering angle. The background, mainly from fragmentation in air, was subtracted. Figure 7 shows the results for $Z = 2$ up to $Z = 7$, including the systematic and statistical uncertainties.

The results were compared to four different nuclear interaction models used in Monte Carlo codes: the Binary Cascade (BIC) model in Geant4, Quantum Molecular Dynamics (QMD) in Geant4, the IntraNuclear Cascade Liége (INCL++) model in Geant4, and FLUKA. The measured differential cross sections together with the predictions of these four models are given in Fig. 7. We see that FLUKA, QMD, and INCL++ are reasonably well reproduced by the data, with INCL++ being the best.

3.3. Towards mass identification

For mass identification, an excellent energy resolution is crucial. The energy resolution of the calorimeter was determined for protons and carbon primary particles of known energy, without a target. For each of the beams, the amplitude distribution of the detected particles was analyzed. The result is given in Fig. 8, where the maximum amplitude spectra are shown for protons and carbon ions of different energies [21]. The response was close to linear with energy, and resolutions were found between 0.3% (carbon) and 2% (protons) [21]. We expect that this is sufficient for mass identification.

4. Conclusions

FOOT is an applied nuclear physics experiment, designed as a compact and portable setup. Two different experimental setups were developed: an electronic setup focused on heavier fragments ($Z \geq 2$) that are forward-peaked, and an emulsion spectrometer setup for lighter fragments ($Z \leq 3$) that spread more widely. The research and development phase is now completed. The FOOT detectors have been constructed and are now being tested. Several future data takings are planned, for example at CNAO at and GSI.

Acknowledgments

We thank GSI, HIT, and CNAO for the successful operation of their facilities during the data taking. The FOOT Collaboration acknowledges INFN for

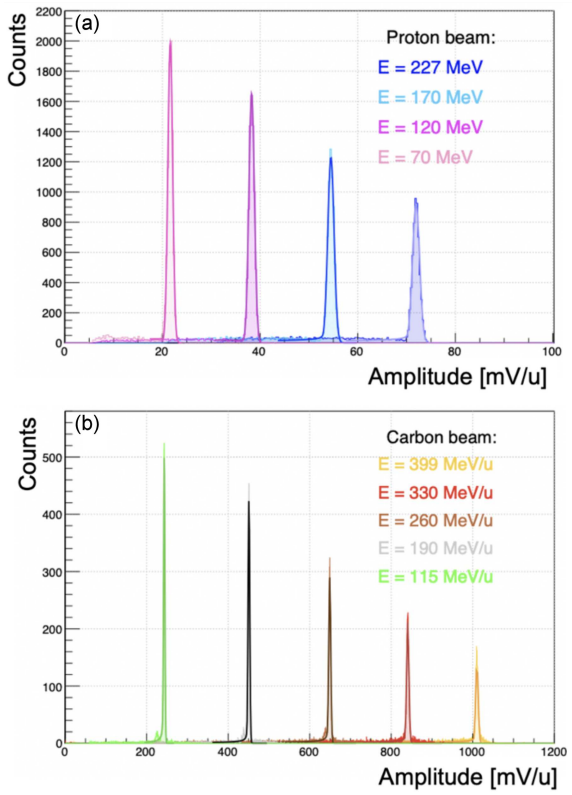

Fig. 8. The maximum amplitude spectra for one of the calorimeter crystals for protons and carbon ions of different energies. Reproduced with permission from [24].

its support in building and running the detector. We also acknowledge the support of the MAECI project *Measuring Oxygen Fragmentation For Improved Ion Therapy Strategies* (CUP I53C2300185000, MAECI Grande Rilevanza Germania, 2023).

References

[1] J.S. Loeffler, M. Durante, *Nat. Rev. Clin. Oncol.* **10**, 411 (2013).

[2] H. Tsujii, T. Kamada, T. Shirai, K. Noda, H. Tsuji, K. Karasawa, *Carbon-Ion Radiotherapy Principles, Practices, and Treatment Planning*, Springer, Tokyo 2014.

[3] M. Durante, H. Paganetti, *Rep. Prog. Phys.* **79**, 096702 (2016).

[4] A. Mairani, S. Mein, E. Blakely et al., *Phys. Med. Biol.* **67**, 15TR02 (2022).

[5] O. Mohamad, J.B. Sishc, J. Saha, A. Pompos, A. Rahimi, M.D. Story, A.J. Davis, D.W.N. Kim, *Cancers* **9**, 66 (2017).

[6] A.C. Kraan, A. Del Guerra, *IEEE Trans. Radiat. Plasma Med. Sci.* **8**, 453 (2024).

[7] F. Tommasino, M. Durante, *Cancers* **7**, 353 (2015).

[8] S. Mein, I. Dokic, C. Klein et al., *Radiat. Oncol.* **14**, 123 (2019).

[9] B. Jones, T.S. Underwood, R.G. Dale, *Br. J. Radiol.* **84**, S61 (2011).

[10] S. Muraro, G. Battistoni, A.C. Kraan, *Front. Phys. Sec. Med. Phys. Imaging* **8**, 567800 (2020).

[11] J. W. Norbury, G. Battistoni, J. Besuglow et al., *Front. Phys. Sec. Med. Phys. Imaging* **8**, 565954 (2020).

[12] F. Luoni, F. Horst, C.A. Reidel et al., *New J. Phys.* **23**, 101201 (2021).

[13] G. Battistoni, M. Toppi, V. Patera et al., *Front. Phys.* **8**, 555 (2021).

[14] G. Galati, V. Boccia, A. Alexandrov et al., *Front. Phys.* **11**, 1327202 (2024).

[15] G. Traini, A. Alexandrov, B. Alpat, *Il Nuovo Cimento* **43C**, 16 (2020).

[16] Y. Dong, S. Gianluigi, C. Sofia et al., *Nucl. Instrum. Methods Phys. Res. A* **986**, 164756 (2021).

[17] A. Trigilio, L. Sabbatini, B. Alpat et al., *J. Instum.* **20**, T09010 (2025).

[18] G. Silvestre, FOOT Collaboration, *Nucl. Instrum. Methods Phys. Res. A* **1047**, 167717 (2023).

[19] M. Morrocchi, E. Ciarrocchi, A. Alexandrov et al., *Nucl. Instrum. Methods Phys. Res. A* **916**, 116 (2019).

[20] A.C. Kraan, R. Zarrella, A. Alexandrov et al., *Nucl. Instrum. Methods Phys. Res. A* **1001**, 165206 (2021).

[21] N. Bartosik, F. Cavanna, L. Ramello et al, *J. Instrum.* **20**, P03021 (2025).

[22] S. Biondi, *IEEE Trans. Nucl. Sci.* **68**, 2464 (2021).

[23] Lorenzo Pierfederici, M.Sc. Thesis, University of Pisa, 2025.

[24] R. Ridolfi, M. Toppi, A. Mengarelli et al., *Phys. Rev. C* **112**, 014610 (2025).